Chiral fermions on lattice axion strings

Srimoyee Sen*

Department of Physics and Astronomy, Iowa State University, Ames, Iowa 50010, USA

(Received 30 July 2022; accepted 22 December 2022; published 13 January 2023)

I discretize axion string configuration coupled to a Dirac fermion, which in the continuum binds a massless chiral fermion in its core when the winding is one. I show that such a configuration can host one or more chiral fermions when regulated on the lattice. To realize these chiral fermions I introduce Wilson-like terms similar to the Wilson term used in lattice domain wall fermions. The number of chiral fermions on the string jumps as the Wilson-like parameter is varied with respect to the other mass scales in the problem. A one-loop Feynman diagram is used to demonstrate how anomaly inflow works in this lattice regularized theory.

DOI: 10.1103/PhysRevD.107.014509

I. INTRODUCTION

In [1], Callan and Harvey demonstrated that fermions coupled to a domain wall in odd number of dimensions and vortex defects in even dimensions $(2n+2)$ can exhibit massless chiral edge states bound to the defects at low energy. For example, the low energy spectrum of a massive Dirac fermion in $2+1$ or $4+1$ dimensions, with a domain wall profile in its mass, has a single chiral fermion bound to the domain wall. Similarly, in the even dimensional case $2n+2$, a Dirac fermion coupled to an axion string exhibits chiral edge states bound to the core of the string. These systems are of interest to both high energy [2–6] and condensed matter physics [7–16].

The chiral edge states living on the defects in both cases suffer from chiral anomaly when fermion number symmetry is gauged and the defect theory by itself violates current conservation. Callan and Harvey showed that current conservation is restored by an inflowing current from the bulk to the defect. This inflowing current can be computed by integrating out the fermion sufficiently far away from the defect where the fermion spectrum is completely gapped.

The continuum construction of chiral fermion edge states on the domain wall was later used by [17] to realize chiral fermions on the lattice. This construction of lattice chiral fermions has the advantage of retaining global chiral symmetry and has therefore been extensively used in simulations of QCD where this is a desirable feature. Interestingly, the construction of a lattice domain wall fermion is more subtle than the continuum construction of Callan-Harvey. The subtleties arise due to the presence of fermion doublers coming from naive discretization of fermions. With naive discretization, the domain wall carries equal numbers of right and left moving doublers which preclude any net chirality on the wall. In order to eliminate the unwanted doublers, one has to use a Wilson-Dirac Lagrangian in a domain wall background for the mass term [17]. For certain values of the Wilson parameter R and the Dirac mass M one can realize a net imbalance of right and left moving modes on the wall resulting in a net chirality.[1] Given the subtleties associated with realization of chiral domain wall fermions, it is interesting to ask how a lattice discretization of axion strings will alter the chiral fermion spectrum confined to the string.

Unsurprisingly, it is not just the lattice theory of domain wall fermions where the presence of fermion doublers eliminates any net chirality on the wall, naive discretization of the axion string theory behaves the same way, i.e., there are equal number of right and left moving doublers on the string. As a result the string carries no net chirality. In order to realize a net chirality on the defect I introduce Wilson-like terms in the Lagrangian to create an imbalance of right and left moving modes on the string. Before discretizing space-time it is convenient to write the axion string in terms of a crossed domain wall configuration as illustrated in the

*srimoyee08@gmail.com

[1]The corresponding bulk theory away from the domain wall exhibits a topological phase analogous to those observed in Chern insulators in condensed matter physics [17–20]. The Wilson parameter in lattice QFT corresponds to the hopping parameter in Chern insulators and the Dirac mass corresponds to magnetic polarization [21,22]. These examples, being demonstrative of the deep ties between lattice fermion field theory and the physics of topological materials, have inspired several papers in recent times [23–29].

next section. This configuration is easier to discretize and the corresponding Wilson-like terms have a simple form. A similar crossed domain wall configuration in the continuum was studied in the context of regulating four dimensional chiral gauge theories in [30].

As shown in Callan-Harvey [1], for domain wall fermions, the fermion number current which flows from the bulk to the boundary in a background electric field (Goldstone-Wilczek current) [31], can be computed using a one-loop Feynman diagram. It was shown [19] that a similar calculation applies for lattice domain wall fermions in the continuum limit, where the Goldstone-Wilczek current is computed using the same Feynman diagram as in the continuum, using lattice perturbation theory. The Feynman diagram on the lattice computes the winding number of a map from momentum space, which on the lattice is a torus, to the Dirac space, which is a sphere. The result therefore is quantized. The winding number of this map jumps as a function of the Dirac mass M and the Wilson parameter R when the bulk fermion propagator goes gapless. As I show in this paper, a similar calculation applies to the axion string. The corresponding Goldstone-Wilczek current is computed using a one-loop Feynman diagram and the net current exhibits discrete jumps as a function of the parameters of the theory just as in lattice domain wall. These discrete changes in the Goldstone-Wilczek current are necessary to compensate for the boundary current as the number and chirality of edge states jump. Furthermore, I find that at certain values of the Wilson-like parameter, the bulk fermion gap goes to zero along a two dimensional surface passing through the defect, coinciding with the discrete jumps in the chiral edge states. This indicates that the discrete jump in chiral edge states is accompanied by a phase transition along this two dimensional surface.

The organization of this paper is as follows. I begin with a brief review of the lattice construction of domain wall fermions which is followed by axion string analysis in the continuum. The subsequent section demonstrates that the axion string configuration is equivalent to a crossed domain wall configuration which is then discretized. The corresponding Wilson-like terms are introduced to engineer chiral edge states on the string and the associated Goldstone-Wilczek current is computed. This is followed by a section which discusses possible numerical realizations of this construction and its relevance to axion insulators.

II. DOMAIN WALL AND VORTEX STRING

To review the lattice domain wall construction, it is convenient to first focus on $2+1$ dimensions (x_0, x_1, x_2) where a Dirac fermion with a mass defect $m = m_0\epsilon(x_2)$ for $m_0 > 0$ exhibits chiral edge states on the defect (domain wall) at $x_2 = 0$. If this fermion theory is discretized naively, the low energy spectrum on the wall will carry equal number of right moving and left moving edge states. This is caused by fermion doubling as can be seen from the discretized Euclidean Dirac equation,

$$\left(-i\gamma^\mu \frac{\sin(p_\mu a)}{a} + \gamma_2 \nabla_2 + m\right)\psi(p, x_2) = 0, \tag{2.1}$$

where μ takes values 0 and 1, the x_0, x_1 coordinates have been Fourier transformed, and ∇_2 is the lattice derivative $\frac{\delta_{x,x+a_2}-\delta_{x,x-a_2}}{2a}$ when the lattice spacing is a. Since I am interested in massless chiral edge states on the wall, I can set $\sum_\mu \gamma_\mu \sin(p_\mu a) = 0$. As seen from this equation, the transverse profile for the states located near the corners of the Brillouin zones $p_0 = n\frac{\pi}{a}$, $p_1 = m\frac{\pi}{a}$ with $n, m = 0, 1$ are identical and all of these modes have normalizable transverse profiles. The modes around the BZ corners $\{0,0\}$ and $\{\frac{\pi}{a}, \frac{\pi}{a}\}$ are of chirality -1 whereas $\{\frac{\pi}{a}, 0\}$ and $\{0, \frac{\pi}{a}\}$ are of chirality $+1$, thus eliminating any net chirality on the wall. It was shown in [17] that one needs to introduce a Wilson term, $\frac{R}{2}\bar{\psi}\nabla^2\psi$ where ∇ is the lattice Laplacian $\nabla = \sum_{\mu=0}^{2} \frac{\delta_{x,x+\mu}+\delta_{x,x-\mu}-2\delta_{x,x}}{a^2}$ in the Lagrangian in order to realize an imbalance between right and left moving modes. To see how this comes about, one can set $R = a$. Then the equation for the transverse profile for the edge states becomes

$$\psi(x_2 + a) = -(m_{\text{eff}})\psi(x_2), \tag{2.2}$$

where $m_{\text{eff}} = ma - 1 - F(p)$ with $F(p) = \sum_{\mu=0,1}(1 - \cos(p_\mu a))$. This equation is solved by the ansatz $\psi = (-m_{\text{eff}})^{x_2/a}$ and a normalizable mode exists as long as

$$2 > m_0 a - F(p) > 0. \tag{2.3}$$

For $0 < m_0 a < 2$, it is only the states around $\{0,0\}$ which are normalizable. For $2 < m_0 a < 4$, the normalizable states are centered around $\{0, \frac{\pi}{a}\}$ and $\{\frac{\pi}{a}, 0\}$. Similarly for $4 < m_0 a < 6$, it is the states centered around $\{\frac{\pi}{a}, \frac{\pi}{a}\}$ which have normalizable solutions. For $m_0 a > 6$ there are no normalizable chiral edge states on the domain wall. If we focus just on the zero modes, we see that their number and chirality jump as a function of the parameter $m_0 a^2/R$ (or $m_0 a$ for $R = a$). The corresponding continuum limit is obtained by taking $a \to 0$ while holding $m_0 a$ constant. It naturally raises the question as to whether the Goldstone-Wilczek current also jumps as a function of $m_0 a$ to account for the current flowing on the boundary as one takes the continuum limit. In order to understand how the Goldstone-Wilczek current compensates for the boundary current, one can gauge the fermion number symmetry and then integrate out the Wilson-Dirac fermion away from the domain wall as shown in [19]. This leaves behind a Chern-Simons theory for the gauge field at low energy. The corresponding

Chern-Simons coefficient is computed using a Feynman integral and can be expressed as

$$c = \frac{-i}{2}\frac{\epsilon_{\mu_0\mu_1\mu_2}}{3!}\int\frac{d^3p}{(2\pi)^3}\mathrm{Tr}\{[S(p)\partial_{\mu_0}S(p)^{-1}][S(p)\partial_{\mu_1}S(p)^{-1}] \times [S(p)\partial_{\mu_2}S(p)^{-1}]\} \tag{2.4}$$

where $S^{-1}(p)$ is the lattice fermion propagator given by

$$S^{-1}(p) = \sum_{\mu=0}^{2} i\frac{\gamma_\mu \sin(p_\mu a)}{a} + m + r\sum_{\mu=1}^{2}[\cos(p_\mu a) - 1] \tag{2.5}$$

and the Chern-Simons effective action is $S_{\text{eff}} = c\epsilon_{\alpha_0\alpha_1\alpha_2}\times \int d^3x A_{\alpha_0}\partial_{\alpha_1}A_{\alpha_2}$. It was explained in [19] that the Feynman integral computes the winding number of a map from a torus (momentum space) to a sphere specified by $S^{-1}(p)$. The Chern-Simons level $4\pi ic$ jumps between 1, −2, and 1 as $m_0 a$ is varied from $0 < m_0 a < 2$, $2 < m_0 a < 4$ and then $4 < m_0 a < 6$ exactly compensating for the current on the wall. These jumps in the Chern-Simons level indicate Chern insulatorlike topological phase transitions within the bulk away from the domain wall.

A. Continuum analysis of axion string

As discussed in Callan-Harvey [1], besides a domain wall in odd dimensional Dirac fermion theories, a Dirac fermion coupled to axion strings in even $2n+2$ dimensional theories can also exhibit chiral edge states. The continuum analysis of this was presented in Callan-Harvey [1] which I briefly review here. I specialize to four dimensions for this discussion. Note that, in this section I will use Minkowski metric while reviewing Callan-Harvey's calculation. When I discuss the lattice theory in Sec. III, I will use Euclidean space-time. The continuum Minkowski Lagrangian for a Dirac fermion coupled to an axion string in four space-time dimensions is given by

$$\mathcal{L} = \bar{\Psi}(i\Gamma^\mu\partial_\mu)\Psi - \bar{\Psi}(\phi_1 - i\phi_2\bar{\Gamma})\Psi, \tag{2.6}$$

where $\bar{\Gamma} = i\Gamma^0\Gamma^1\Gamma^2\Gamma^3$. Here $\phi_1 + i\phi_2 \equiv \phi$ is the vacuum expectation value of a complex scalar field, the phase fluctuations of which correspond to an axion field. Since I am interested in static axion string configuration, I can take the phase to wind by 2π around the x^1 axis without a loss of generality. To find the low energy spectrum on the string I can now write the equation of motion for the fermion field in the background of axion string as

$$(i\Gamma^\mu\partial_\mu)\Psi = (\phi_1 - i\phi_2\bar{\Gamma})\Psi. \tag{2.7}$$

To look for a massless chiral fermion solution to the equation of motion (EOM), I set $\partial_0 = \partial_1 = 0$, and obtain

$$(i\Gamma^2\partial_2 + i\Gamma^3\partial_3)\Psi = (\phi_1 - i\phi_2\bar{\Gamma})\Psi. \tag{2.8}$$

I make a specific choice for gamma matrices for convenience with $\Gamma^0 = \sigma_1 \otimes \sigma_0$ where σ_0 is the two dimensional identity matrix and $\Gamma^i = i\sigma_2 \otimes \sigma_i$. Writing this equation in polar coordinates, $x^2 = r\cos\theta$, $x^3 = r\sin\theta$, I look for θ independent solutions with $\partial_{x^2} = \cos\theta\partial_r$, $\partial_{x^3} = \sin\theta\partial_r$. Thus, the EOM reduces to

$$\begin{pmatrix} 0 & 0 & i\sin\theta & \cos\theta \\ 0 & 0 & -\cos\theta & -i\sin\theta \\ -i\sin\theta & -\cos\theta & 0 & 0 \\ \cos\theta & i\sin\theta & 0 & 0 \end{pmatrix}\partial_r\begin{pmatrix}\Psi_+\\ \Psi_-\end{pmatrix} = f(r)\begin{pmatrix} e^{i\theta} & 0 & 0 & 0 \\ 0 & e^{i\theta} & 0 & 0 \\ 0 & 0 & e^{-i\theta} & 0 \\ 0 & 0 & 0 & e^{-i\theta}\end{pmatrix}\begin{pmatrix}\Psi_+\\ \Psi_-\end{pmatrix}. \tag{2.9}$$

Here I have used

$$\Psi = \begin{pmatrix}\Psi_+\\ \Psi_-\end{pmatrix}$$

and $\phi = f(r)e^{i\theta}$ where r is the radial distance from the center of the string and $f(r) = |\phi|$ is only a function of the radial coordinate. The phase of the scalar field winds uniformly around the x^1 axis which produces the corresponding azimuthal angular dependence of $e^{i\theta}$. This equation is solved by the following ansatz:

$$\begin{pmatrix}0\\ \Psi_-\end{pmatrix} = \eta e^{-\int_0^\rho f(\sigma)d\sigma}$$
$$\begin{pmatrix}\Psi_+\\ 0\end{pmatrix} = -i\Gamma_2\begin{pmatrix}0\\ \Psi_-\end{pmatrix} = -i\Gamma_2\eta e^{-\int_0^\rho f(\sigma)d\sigma}, \tag{2.10}$$

where $\Gamma_{\text{int}}\eta = -\eta$, $\bar{\Gamma}\eta = \eta$, and Γ_{int} measures the chirality of the solution with $\Gamma_{\text{int}} = -\Gamma^0\Gamma^1$. For the particular choice of gamma matrices here, one can rewrite the solution as

$$\begin{pmatrix}\Psi_+\\ \Psi_-\end{pmatrix} = \begin{pmatrix}-1\\ 1\\ 1\\ 1\end{pmatrix}e^{-\int f(\sigma)d\sigma}. \tag{2.11}$$

Clearly this massless chiral fermion suffers from anomaly which leads to nonconservation of fermion number current on the string in a background electric field. This is remedied by the inflowing Goldstone-Wilczek current which can be computed in perturbation theory away from the vortex core. To do this computation I parametrize $\phi_1 + i\phi_2$ as $(v + \delta v)e^{i\alpha}$ where δv and α vary slowly in space. I can then expand the Lagrangian in α and δv to get

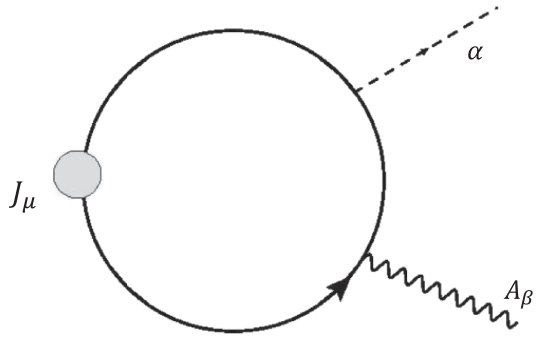

FIG. 1. The one-loop Feynman diagram for the Goldstone-Wilczek current.

$$\mathcal{L} = \bar{\Psi}(i\Gamma^\mu \partial_\mu - v)\Psi + i\alpha v \bar{\Psi}\bar{\Gamma}\Psi - \delta v \bar{\Psi}\Psi + \cdots. \quad (2.12)$$

I can now attempt to compute the Goldstone Wilczek current by treating δv and α as perturbation. The corresponding fermion propagator in momentum space is given by

$$S_F = \frac{i(\Gamma_\mu p^\mu + f)}{p^2 - f^2 + i\epsilon}. \quad (2.13)$$

Gauging the fermion number symmetry, the fermion number current can be computed up to leading order in $\frac{\partial_\sigma \alpha}{f}$ using the Feynman diagram in Fig. 1 as [1],

$$\mathcal{J}^\mu = \langle \bar{\Psi}\Gamma_\mu \Psi \rangle = -\frac{1}{8\pi^2}\epsilon^{\mu\nu\beta\sigma} F_{\nu\beta}\partial_\sigma \alpha. \quad (2.14)$$

A chiral edge state of negative chirality on the string carries a current of $-\frac{E_1}{2\pi}$ when an electric field E_1 is applied in the direction of the string. To see how current conservation works, I can substitute the smooth axion string (vortex) configuration with $\alpha = \theta$ where θ is the azimuthal coordinate $\theta = \tan^{-1}(\frac{x^3}{x^2})$. For this field configuration all components of the current density in Eq. (2.14) is zero except the radial component. The net current flowing to the string is then given by

$$\int \mathcal{J}_r (r d\theta) = -\frac{1}{2\pi} E_1 \quad (2.15)$$

compensating for the current flowing on the string.

B. Crossed domain wall

Before I discuss the lattice construction of axion string edge states, I will in this section demonstrate that an axion string configuration in the continuum can be deformed into a crossed domain wall configuration. The motivation to relate the two configurations arises from the observation that the crossed domain wall is relatively easy to discretize. As I will show, the crossed domain wall carries the same winding as the vortex configuration and hosts a chiral edge state confined to it. The latter is not surprising since the configurations carry the same winding in $\phi_1 + i\phi_2$. The Goldstone-Wilczek current is only sensitive to this winding, ensuring that the low energy fermion spectrum of the two configurations match. The crossed domain wall configuration I will consider will involve a domain wall in the field ϕ_1 and another in ϕ_2. Note the most general form for the crossed domain wall configuration is

$$\phi_1 = m_1 \epsilon(x^2) + \delta m_1, \qquad \phi_2 = m_2 \epsilon(x^3) + \delta m_2 \quad (2.16)$$

with $m_1 > \delta m_1 > 0$, $m_2 > \delta m_2 > 0$. As we will see, the hierarchy between m_1 and δm_1 as well as m_2 and δm_2, is important in order to obtain a nontrivial winding and a localized chiral edge state. If the hierarchy is reversed as in $\delta m_1 > m_1$ or $\delta m_2 > m_2$, the chiral edge state is lost and the winding of the domain wall configuration goes to zero. If I define angular coordinate θ such that the four quadrants $\{x_2 > 0, x_3 > 0\}$, $\{x_2 < 0, x_3 > 0\}$, $\{x_2 < 0, x_3 < 0\}$, and $\{x_2 > 0, x_3 < 0\}$ map to $\frac{\pi}{2} > \theta > 0$, $\pi > \theta > \frac{\pi}{2}$, $\frac{3\pi}{2} > \theta > \pi$, and $2\pi > \theta > \frac{3\pi}{2}$, then I can write

$$\phi_1 = m_1 \frac{\cos\theta}{|\cos\theta|} + \delta m_1, \quad (2.17)$$

$$\phi_2 = m_2 \frac{\sin\theta}{|\sin\theta|} + \delta m_2. \quad (2.18)$$

I can reparametrize $\phi_1 + i\phi_2 = h(\cos\alpha + i\sin\alpha)$ such that

$$\tan\alpha = \frac{m_2 \frac{\sin\theta}{|\sin\theta|} + \delta m_2}{m_1 \frac{\cos\theta}{|\cos\theta|} + \delta m_1}, \quad (2.19)$$

$$h = \sqrt{\left(m_1 \frac{\cos\theta}{|\cos\theta|} + \delta m_1\right)^2 + \left(m_2 \frac{\sin\theta}{|\sin\theta|} + \delta m_2\right)^2}. \quad (2.20)$$

Denoting $\alpha(\theta = 0) \equiv \alpha_0$, it is easy to see that as θ is varied from 0 to 2π, α goes from α_0 to $\alpha_0 + 2\pi$ as long as $m_1 > \delta m_1$, $m_2 > \delta m_2$. Then, α winds in the azimuthal direction just as one expects in a vortex. In other words

$$\int_0^{2\pi} \frac{1}{r}(\partial_\theta \alpha) r d\theta = \int_{\alpha_0}^{\alpha_0 + 2\pi} d\alpha = 2\pi. \quad (2.21)$$

Of course I can choose to deform the crossed domain wall profiles slightly by replacing the step functions $\epsilon(x_2)$ and $\epsilon(x_3)$ by $\tanh(x_2)$ and $\tanh(x_3)$. This however does not affect the winding of α. In fact, the vortex configuration used in the previous section $f(\rho)e^{i\theta}$ can simply be deformed into a crossed domain wall configuration by

choosing $\delta m_1 = \delta m_2 = 0$ and $m_1 = m_2 = f(\rho \to \infty)$. In this case we have $\tan(\alpha) = \frac{\tan(\theta)}{|\tan\theta|}$ and $h = f(\infty)$.

I will now look for chiral edge state solutions confined to the crossed domain wall defect. For this I consider the equation of motion of the fermion coupled to this crossed domain wall, setting $\partial_0 = \partial_1 = 0$

$$\begin{pmatrix} 0 & 0 & i\partial_3 & \partial_2 \\ 0 & 0 & -\partial_2 & -i\partial_3 \\ -i\partial_3 & -\partial_2 & 0 & 0 \\ \partial_2 & i\partial_3 & 0 & 0 \end{pmatrix} \begin{pmatrix} \Psi_+ \\ \Psi_- \end{pmatrix} = \begin{pmatrix} m & 0 & 0 & 0 \\ 0 & m & 0 & 0 \\ 0 & 0 & m^* & 0 \\ 0 & 0 & 0 & m^* \end{pmatrix} \begin{pmatrix} \Psi_+ \\ \Psi_- \end{pmatrix} \tag{2.22}$$

where I have used $m = m_1\epsilon(x^2) + \delta m_1 + i(m_2\epsilon(x^3) + \delta m_2)$. Defining $\pm m_1 + \delta m_1 = m_1^{\pm}$, $\pm m_2 + \delta m_2 = m_2^{\pm}$ it is easy to see that this equation is solved by

$$\begin{pmatrix} \Psi_+ \\ \Psi_- \end{pmatrix} = \begin{pmatrix} -1 \\ 1 \\ 1 \\ 1 \end{pmatrix} \kappa(x_2, x_3) \tag{2.23}$$

where

$$\kappa = e^{-m_1^+ x^2 - m_2^+ x^3}\theta(x^2)\theta(x^3) + e^{-m_1^- x^2 - m_2^+ x^3}\theta(-x^2)\theta(x^3) + e^{-m_1^- x^2 - m_2^- x^3}\theta(-x^2)\theta(-x^3) + e^{-m_1^+ x^2 - m_2^- x^3}\theta(x^2)\theta(-x^3). \tag{2.24}$$

Again, note that the solution is normalizable only when $m_1 > \delta m_1 > 0$, $m_2 > \delta m_2 > 0$. In the limit of $\delta m_1 = \delta m_2 = 0$ and $m_1 = m_2 = f_\infty$, the solution is

$$\kappa = e^{-f_\infty(|x_2| + |x_3|)}. \tag{2.25}$$

We therefore see that a crossed domain wall configuration carries the same winding number as in the axion string configuration. The massless edge state spectrum of the two defects are also identical, there being a chiral edge state of the same chirality confined to the core in both cases.

III. DISCRETIZING SPACE-TIME

I now consider the crossed domain wall on discrete Euclidean space-time and look for chiral edge states. I choose a square lattice such that a^μ, the lattice spacing in x^μ direction, is $a^\mu = a$. The equation of motion for the fermion in the background of a domain wall with naive discretization looks like

$$-\frac{i\Gamma_\mu^E \sin(p_\mu a)}{a}\Psi + (\Gamma_2^E\nabla_2 + \Gamma_3^E\nabla_3)\Psi = -(\phi_1 - i\phi_2\bar{\Gamma})\Psi, \tag{3.1}$$

where Γ_μ^E are Euclidean gamma matrices $\Gamma_0^E = \Gamma^0$, $\Gamma_i^E = -i\Gamma^i$, ∇_2, ∇_3 are lattice derivatives given by

$$\nabla_{2/3} = \frac{\delta_{x,x+a_{2/3}} - \delta_{x,x-a_{2/3}}}{2a_{2/3}}, \tag{3.2}$$

and the variable μ takes values 0, 1. Note that $\bar{\Gamma}$ is defined in the text below Eq. (2.6). Again I have Fourier transformed the coordinates x_0 and x_1. In order to solve for massless states, I can expand the momenta around the corners of the Brillouin zone (BZ), i.e., $\{p_0 a = 0, p_1 a = 0\}$, $\{p_0 a = 0, p_1 a = \pi\}$, $\{p_0 a = \pi, p_1 a = 0\}$, and $\{p_0 a = \pi, p_1 a = \pi\}$. With an ansatz of the form

$$\psi = \begin{pmatrix} -1 \\ 1 \\ 1 \\ 1 \end{pmatrix} \varphi(p_0, p_1)\chi(x_2, x_3), \tag{3.3}$$

the equation for the transverse profile is

$$\nabla_2\chi = -\phi_1\chi \Rightarrow \chi(x_2 + a) - \chi(x_2 - a) = -2a\phi_1\chi(x_2),$$
$$\nabla_3\chi = -\phi_2\chi \Rightarrow \chi(x_3 + a) - \chi(x_3 - a) = -2a\phi_2\chi(x_3). \tag{3.4}$$

These two equations are solved by $\chi(x_2, x_3) = z_2^{x_2} z_3^{x_3}$ where

$$z_{2/3} = \frac{-2a\phi_{1/2} - \sqrt{4a^2\phi_{1/2}^2 + 4}}{2}. \tag{3.5}$$

So, it is clear that the conditions of normalizability for all the doublers are the same and as a result we do not have a net chirality on the string. In order to engineer net chirality on the string I will have to introduce Wilson-like terms in the Lagrangian. For this purpose, I propose adding to the Euclidean Lagrangian the following terms: $\frac{R}{2}\bar{\Psi}(\nabla_2^2 + \nabla_{\text{int}}^2)\Psi - i\frac{R}{2}\bar{\Psi}\bar{\Gamma}(\nabla_3^2 + \nabla_{\text{int}}^2)\Psi$ where $\nabla_{\text{int}}^2 = \nabla_0^2 + \nabla_1^2$. This shifts ϕ_1 to $\phi_1 + \frac{R}{2a^2}(\nabla_2^2 + \nabla_{\text{int}}^2)$ and ϕ_2 to $\phi_2 + \frac{R}{2a^2}(\nabla_3^2 + \nabla_{\text{int}}^2)$. Thus the equation of motion with an ansatz as in Eq. (3.3) is

$$\nabla_2\chi = -\left(\phi_1 + \frac{R}{2}\nabla_2^2 + \frac{R}{2a^2}\sum_\mu(2\cos(p_\mu a) - 2)\right)\chi,$$
$$\nabla_3\chi = -\left(\phi_2 + \frac{R}{2}\nabla_3^2 + \frac{R}{2a^2}\sum_\mu(2\cos(p_\mu a) - 2)\right)\chi. \tag{3.6}$$

TABLE I. Number and chirality of edge states.

	$2>m_1a>0$	$4>m_1a>2$	$6>m_1a>4$	$m_1a>6$
$2>m_2a>0$	-1	0	0	0
$4>m_2a>2$	0	2	0	0
$6>m_2a>4$	0	0	-1	0
$m_2a>6$	0	0	0	0

I set $R=a$, and solve for the transverse profile with the same ansatz as before, i.e.,

$$\chi(x_2,x_3)=z_2^{x_2}z_3^{x_3}. \tag{3.7}$$

The solutions are given by[2]

$$z_2^a=-\left(a\phi_1-1+\sum_{\mu=0,1}(\cos(p_\mu a)-1)\right),$$
$$z_3^a=-\left(a\phi_2-1+\sum_{\mu=0,1}(\cos(p_\mu a)-1)\right). \tag{3.8}$$

I now impose $\delta m_1=0$ and $\delta m_2=0$ and obtain the condition of normalizability for the different doublers. If I focus on the corners of the BZ, the mode $\{p_0=0,p_1=0\}$ is normalizable for $0<m_1a<2$ and $0<m_2a<2$. The modes $\{p_0=0,p_1=\frac{\pi}{a}\}$ and $\{p_0=\frac{\pi}{a},p_1=0\}$ are normalizable for $2<m_1a<4$ and $2<m_2a<4$. Similarly, the mode $\{p_0=\frac{\pi}{a},p_1=\frac{\pi}{a}\}$ is normalizable for $4<m_1a<6$ and $4<m_2a<6$. There are no normalizable solutions for $m_{1/2}a>6$. I list the number and chirality of normalizable edge state solutions in Table I for various values of the parameters m_1a and m_2a. In Fig. 2, I plot the values of the parameters for which one finds chiral edge states solutions on the crossed domain wall defect.

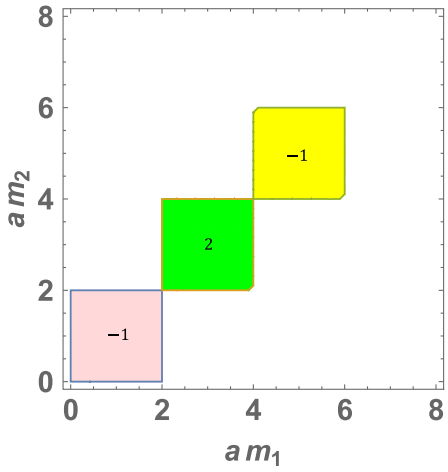

FIG. 2. The light red, green, and yellow regions indicate the values of the parameters of the crossed domain wall, m_1 and m_2, for which there exist chiral edge states. The net chirality for the relevant parameters is also indicated inside the colored regions. In the region outside of the colored boxes, there are no chiral edge states confined to the defect.

A. Goldstone-Wilczek current

Having obtained the edge state solutions for the crossed domain wall configuration on the lattice, I will now proceed to compute the Goldstone-Wilczek current while taking the continuum limit. I will begin with the Euclidean lattice Lagrangian

$$\mathcal{L}_E=\bar\Psi(\Gamma_\mu^E\nabla_\mu)\Psi+\bar\Psi\left(\phi_1+\frac{R}{2a^2}(\nabla_2^2+\nabla_{\rm int}^2)\right)\Psi$$
$$-i\bar\Psi\bar\Gamma\left(\phi_2+\frac{R}{2a^2}(\nabla_3^2+\nabla_{\rm int}^2)\right)\Psi. \tag{3.9}$$

At this point I will partition this Lagrangian in two parts and discuss them in order:

$$\mathcal{L}_E=\mathcal{L}_E^1+\mathcal{L}_E^2, \tag{3.10}$$

where

$$\mathcal{L}_E^1=\bar\Psi(\Gamma_\mu^E\nabla_\mu)\Psi+\frac{R}{2a^2}\bar\Psi(\nabla_2^2+\nabla_{\rm int}^2)\Psi$$
$$-i\frac{R}{2a^2}\bar\Psi\bar\Gamma(\nabla_3^2+\nabla_{\rm int}^2)\Psi \tag{3.11}$$

contains the kinetic term and the Wilson-like term whereas

$$\mathcal{L}_E^2=\phi_1\bar\Psi\Psi-i\phi_2\bar\Psi\bar\Gamma\Psi \tag{3.12}$$

contains the two mass terms involving ϕ_1 and ϕ_2. Let us first consider $\mathcal{L}_E^1$. In momentum space I can write the corresponding action as

$$\mathcal{S}_E^1=\int\frac{d^4p}{(2\pi)^4}\left[\bar\Psi(p)\left(-i\Gamma_\mu^E\frac{\sin(ap_\mu)}{a}\right)\Psi(p)\right.$$
$$+\bar\Psi(p)\left(\frac{R}{a^2}\sum_{i=0,1,2}(\cos(p_ia)-1)\right)\Psi(p)$$
$$\left.-i\bar\Psi(p)\bar\Gamma\left(\frac{R}{a^2}\sum_{i=0,1,3}(\cos(p_ia)-1)\right)\Psi(p)\right]. \tag{3.13}$$

The momentum integration in Eq. (3.13) is over one Brillouin zone. It is convenient to divide the momentum space integral around the BZ corners. Let us denote the

[2]Note that one could instead introduce a standard Wilson term $\frac{R}{2}\bar\Psi\nabla^2\Psi$ and engineer chiral edge states by tuning ϕ_1, ϕ_2, and R appropriately. In this case the equation of motion takes the form $\nabla_2\chi=-(\phi_1+\frac{R}{2}\nabla_2^2+\frac{R}{2}\nabla_3^2+\frac{R}{2a^2}\sum_\mu(2\cos(p_\mu a)-2))\chi$, $\nabla_3\chi=-\phi_2\chi$. The analysis of these equations and the corresponding Goldstone-Wilczek current is slightly more subtle and I leave it for future work.

fermion field $\Psi(p)$ near the BZ corner $p = \frac{\pi}{a}\{i,j,k,l\}$ as $\psi_{i,j,k,l}$ where i,j,k,l can either be 0 or 1. I can now split the action over momentum integrals around the BZ corners by expanding in small p as

$$\mathcal{S}_{\rm E}^1 = -\int \sum_{i,j,k,l} \bar{\psi}_{i,j,k,l}(p)(i(-1)^i\delta_{\mu,0}\Gamma_\mu^E p_\mu + i(-1)^j\delta_{\mu,1}\Gamma_\mu^E p_\mu + i(-1)^k\delta_{\mu,2}\Gamma_\mu^E p_\mu + i(-1)^l\delta_{\mu,3}\Gamma_\mu^E p_\mu)\psi_{i,j,k,l}(p)$$
$$+ \int \sum_{i,j,k,l} \bar{\psi}_{i,j,k,l}(p)\left[\left(-2\frac{R}{a^2}\delta_{i,1} - 2\frac{R}{a^2}\delta_{j,1} - 2\frac{R}{a^2}\delta_{k,1}\right) - i\bar{\Gamma}\left(-2\frac{R}{a^2}\delta_{i,1} - 2\frac{R}{a^2}\delta_{j,1} - 2\frac{R}{a^2}\delta_{l,1}\right)\right]\psi_{i,j,k,l}(p). \quad (3.14)$$

Thus I have rewritten the Lagrangian in terms of 16 flavors of fermions. I can redefine the gamma matrices for these different flavors so as to absorb the factor of $(-1)^{i/j/k/l}$ in the definition of the gamma matrices using similarity transformation. The redefined gamma matrices for the flavor $\{i,j,k,l\}$ are given by

$$P_{i,j,k,l}\Gamma_0^E P_{i,j,k,l}^{-1} = (-1)^i\Gamma_0^E, \qquad P_{i,j,k,l}\Gamma_1^E P_{i,j,k,l}^{-1} = (-1)^j\Gamma_1^E,$$
$$P_{i,j,k,l}\Gamma_2^E P_{i,j,k,l}^{-1} = (-1)^k\Gamma_2^E, \qquad P_{i,j,k,l}\Gamma_3^E P_{i,j,k,l}^{-1} = (-1)^l\Gamma_3^E. \quad (3.15)$$

This similarity transform takes the $\bar{\Gamma}$ matrix to

$$\bar{\Gamma}^{i,j,k,l} = (-1)^{i+j+k+l}\bar{\Gamma}. \quad (3.16)$$

Therefore the action reduces to

$$\mathcal{S}_{\rm E}^1 = \int \sum_{i,j,k,l} \bar{\psi}_{i,j,k,l}(p)\left[-i\Gamma_\mu^E p_\mu + \left(-2\frac{R}{a^2}\delta_{i,1} - 2\frac{R}{a^2}\delta_{j,1} - 2\frac{R}{a^2}\delta_{k,1}\right)\right]\psi_{i,j,k,l}(p)$$
$$- \int \sum_{i,j,k,l} \bar{\psi}_{i,j,k,l}(p)\left[i\bar{\Gamma}^{i,j,k,l}\left(-2\frac{R}{a^2}\delta_{i,1} - 2\frac{R}{a^2}\delta_{j,1} - 2\frac{R}{a^2}\delta_{l,1}\right)\right]\psi_{i,j,k,l}(p). \quad (3.17)$$

Fourier transforming back to position space I rewrite this action as

$$\mathcal{S}_{\rm E}^1 = \int \sum_{i,j,k,l} \bar{\psi}_{i,j,k,l}(x)\left[\Gamma_\mu^E\partial_\mu + \left(-2\frac{R}{a^2}\delta_{i,1} - 2\frac{R}{a^2}\delta_{j,1} - 2\frac{R}{a^2}\delta_{k,1}\right)\right]\psi_{i,j,k,l}(x)$$
$$- \int \sum_{i,j,k,l} \bar{\psi}_{i,j,k,l}(x)\left[i\bar{\Gamma}^{i,j,k,l}\left(-2\frac{R}{a^2}\delta_{i,1} - 2\frac{R}{a^2}\delta_{j,1} - 2\frac{R}{a^2}\delta_{l,1}\right)\right]\psi_{i,j,k,l}(x). \quad (3.18)$$

Let us now consider the second piece of the Lagrangian $\mathcal{L}_{\rm E}^2$. When I transform to momentum space the corresponding action integral can be written as

$$\mathcal{S}_{\rm E}^2 = \int \frac{d^4p}{(2\pi)^4}\int \frac{d^4k}{(2\pi)^4}\bar{\Psi}(p)(\phi_1(p-k) - i\bar{\Gamma}\phi_2(p-k))\Psi(k). \quad (3.19)$$

I can again expand p and k about the corners of the BZ assuming that the spatial variation in ϕ_1 and ϕ_2 takes place over length scales much longer than the lattice spacing. This is achievable by giving the domain walls some width larger than the lattice spacing. I can now write $p = Q + \delta p$ and $k = Q + \delta k$ where Q stands for the momentum corresponding to the BZ corner. Then the action of Eq. (3.19) splits into 16 flavor pieces with

$$\mathcal{S}_{\rm E}^2 = \sum_{i,j,k,l}\int \frac{d^4\delta p}{(2\pi)^4}\int \frac{d^4\delta k}{(2\pi)^4}\bar{\Psi}_{i,j,k,l}(\delta p)(\phi_1(\delta p - \delta k) - i\bar{\Gamma}\phi_2(\delta p - \delta k))\Psi_{i,j,k,l}(\delta k). \quad (3.20)$$

In coordinate space, this action turns into

$$\mathcal{S}_{\rm E}^2 = \sum_{i,j,k,l}\int d^4x\bar{\Psi}_{i,j,k,l}(x)(\phi_1(x) - i\bar{\Gamma}\phi_2(x))\Psi_{i,j,k,l}(x). \quad (3.21)$$

I can now proceed to compute the vector current for the lattice Lagrangian of Eq. (3.9) in the presence of a background gauge field in a crossed domain wall profile for ϕ_1 and ϕ_2. In order to compute this I combine the actions in (3.18) and (3.21)

$$\mathcal{S}_{\mathrm{E}}=\int d^4x\sum_{i,j,k,l}\bar{\psi}_{i,j,k,l}\left[\Gamma^E_\mu\partial_\mu+\left(\phi_1-2\frac{R}{a^2}\delta_{i,1}-2\frac{R}{a^2}\delta_{j,1}-2\frac{R}{a^2}\delta_{k,1}\right)-i\bar{\Gamma}^{i,j,k,l}\left(\phi_2-2\frac{R}{a^2}\delta_{i,1}-2\frac{R}{a^2}\delta_{j,1}-2\frac{R}{a^2}\delta_{l,1}\right)\right]\psi_{i,j,k,l}. \tag{3.22}$$

For every flavor of fermion I can combine the Wilson-like terms and the fermion-scalar coupling to rewrite the action as

$$\mathcal{S}_{\mathrm{E}}=\int\sum_{i,j,k,l}\bar{\psi}_{i,j,k,l}(\Gamma^E_\mu\partial_\mu)\psi_{i,j,k,l}+\int\sum_{i,j,k,l}f_{i,j,k,l}\bar{\psi}_{i,j,k,l}\psi_{i,j,k,l}-i\int\sum_{i,j,k,l}(-1)^{i+j+k+l}\theta_{i,j,k,l}f_{i,j,k,l}\bar{\psi}_{i,j,k,l}\bar{\Gamma}\psi_{i,j,k,l} \tag{3.23}$$

where

$$f_{i,j,k,l}\equiv\sqrt{\left(\phi_1-2\frac{R}{a^2}\delta_{i,1}-2\frac{R}{a^2}\delta_{j,1}-2\frac{R}{a^2}\delta_{k,1}\right)^2+\left(\phi_2-2\frac{R}{a^2}\delta_{i,1}-2\frac{R}{a^2}\delta_{j,1}-2\frac{R}{a^2}\delta_{l,1}\right)^2} \tag{3.24}$$

and

$$\theta_{i,j,k,l}=\tan^{-1}\left((-1)^{i+j+k+l}\left(\frac{\phi_2-2\frac{R}{a^2}\delta_{i,1}-2\frac{R}{a^2}\delta_{j,1}-2\frac{R}{a^2}\delta_{l,1}}{\phi_1-2\frac{R}{a^2}\delta_{i,1}-2\frac{R}{a^2}\delta_{j,1}-2\frac{R}{a^2}\delta_{k,1}}\right)\right). \tag{3.25}$$

This now looks like 16 copies of the continuum Callan-Harvey Lagrangian with 16 different spatially varying mass terms. Now I set $R=a$ as before. For each flavor of fermion, I can now compute the current, treating $\theta_{i,j,k,l}$ as a background field while writing the fermion propagator as

$$S_{i,j,k,l}=\frac{(\Gamma^E_\mu p_\mu+f_{i,j,k,l})}{p^2+f^2_{i,j,k,l}} \tag{3.26}$$

and using the same Feynman diagram as in Fig. 1. For $f_{i,j,k,l}\gg\partial_\nu\theta_{i,j,k,l}$, up to leading order in $\frac{\partial_\nu\theta_{i,j,k,l}}{f_{i,j,k,l}}$ expansion, the current for the flavor $\{i,j,k,l\}$ is given by

$$\mathcal{J}^{i,j,k,l}_\mu=-\frac{\epsilon_{\mu\nu\lambda\rho}}{8\pi^2}\partial_\nu\theta_{i,j,k,l}F^{\lambda\rho} \tag{3.27}$$

which leads to the net current

$$\mathcal{J}_\mu=\sum_{i,j,k,l}\mathcal{J}^{i,j,k,l}_\mu=-\sum_{i,j,k,l}\frac{\epsilon_{\mu\nu\lambda\rho}}{8\pi^2}\partial_\nu\theta_{i,j,k,l}F^{\lambda\rho}. \tag{3.28}$$

Given this expression for the current I can now verify if the integral of the divergence of this current is consistent with the number of chiral edge states on the string so as to ensure current conservation. In order to compute the net current flowing to the string from the bulk, I need to first obtain the various windings seen by the different flavors, i.e., in $\theta_{i,j,k,l}$. Note that the overall sign of the winding will depend on the factor of $(-1)^{i+j+k+l}$ appearing in the definition $\theta_{i,j,k,l}$ in Eq. (3.25). The winding in $\theta_{i,j,k,l}$ for a particular flavor can be obtained by computing

$$\frac{1}{2\pi}\int_0^{2\pi}\frac{1}{r}(\partial_\theta\theta_{i,j,k,l})r\,d\theta \tag{3.29}$$

which is always an integer. For a crossed domain wall configuration the result is a function of the domain wall heights $a|\phi_1|$ and $a|\phi_2|$. As an example let us consider $m_1=m_2=m$ and $\delta m_1=\delta m_2=0$. The corresponding windings for the different flavors are shown in Table II. For $0<am<2$, a winding of 1 is found for the flavor $\psi_{0,0,0,0}$. The winding is zero for all the other flavors. Therefore the net current is

TABLE II. Winding in $\theta_{i,j,k,l}$ as a function of the parameter ma for the 16 different flavors. These windings are used to compute the net radial Goldstone-Wilczek current.

$\{i,j,k,l\}$	$2>ma>0$	$4>ma>2$	$6>ma>4$	$ma>6$
$\{0,0,0,0\}$	1	1	1	1
$\{1,0,0,0\}$	0	−1	−1	−1
$\{0,1,0,0\}$	0	−1	−1	−1
$\{0,0,1,0\}$	0	−1	−1	−1
$\{0,0,0,1\}$	0	−1	−1	−1
$\{1,1,0,0\}$	0	0	1	1
$\{0,1,1,0\}$	0	0	1	1
$\{0,0,1,1\}$	0	1	1	1
$\{1,0,1,0\}$	0	0	1	1
$\{0,1,0,1\}$	0	0	1	1
$\{1,0,0,1\}$	0	0	1	1
$\{1,1,1,0\}$	0	0	0	−1
$\{1,1,0,1\}$	0	0	0	−1
$\{1,0,1,1\}$	0	0	−1	−1
$\{0,1,1,1\}$	0	0	−1	−1
$\{1,1,1,1\}$	0	0	0	1

$$\int rd\theta \sum_{i,j,k,l} \mathcal{J}_r^{i,j,k,l} = -\frac{E_1}{2\pi}. \tag{3.30}$$

This result is consistent with there being one normalizable chiral zero mode of chirality -1 on the string corresponding to $\{p_0 = 0, p_1 = 0\}$ for $0 < am < 2$ as can be seen from Eq. (3.8) or Table I. For $2 < am < 4$ the flavors $\psi_{0,0,0,0}$ and $\psi_{0,0,1,1}$ see a winding of $+1$ whereas the flavors $\psi_{1,0,0,0}$, $\psi_{0,1,0,0}$, $\psi_{0,0,1,0}$, $\psi_{0,0,0,1}$ see a winding of -1. The rest of the flavors do not see any winding. Therefore the net current is

$$\int rd\theta \sum_{i,j,k,l} \mathcal{J}_r^{i,j,k,l} = \frac{E_1}{\pi}. \tag{3.31}$$

This is consistent with the fact that for $2 < am < 4$, there are two $+1$ chirality modes on the wall, i.e., $\{p_0 = 0, p_1 = \frac{\pi}{a}\}$ and $\{p_0 = \frac{\pi}{a}, p_1 = 0\}$. Similarly, for $4 < am < 6$, there are seven flavors which see a positive winding of $+1$. These are $\psi_{0,0,0,0}$, $\psi_{0,0,1,1}$, $\psi_{0,1,1,0}$, $\psi_{1,1,0,0}$, $\psi_{1,0,0,1}$, $\psi_{0,1,0,1}$, $\psi_{1,0,1,0}$. Similarly, there are six flavors which see a winding of -1 and these are $\psi_{1,0,0,0}$, $\psi_{0,1,0,0}$, $\psi_{0,0,1,0}$, $\psi_{0,0,0,1}$, $\psi_{0,1,1,1}$, $\psi_{1,0,1,1}$. The other flavors do not see any net winding. Therefore the net current for this case is

$$\int rd\theta \sum_{i,j,k,l} \mathcal{J}_r^{i,j,k,l} = -\frac{E_1}{2\pi}. \tag{3.32}$$

This current is consistent with there being a single normalizable chiral zero mode of -1 chirality on the string, i.e., the mode $\{p_1 = \frac{\pi}{a}, p_4 = \frac{\pi}{a}\}$. For $am > 6$, all the 16 flavors see a winding, with eight of them seeing a winding of $+1$ and the rest -1. Therefore the net current is zero which is consistent with there being no normalizable edge states for $ma > 6$. In Table III I list the Goldstone-Wilczek current as a function of the parameter ma for the crossed domain wall configuration.

B. Crossed domain wall with unequal domain wall heights

In the previous discussion I concentrated on $m_1 = m_2 = m$ and $\delta m_1 = \delta m_2 = 0$. One can repeat the analysis of the Goldstone-Wilczek current relaxing these conditions and it is easy to see that the corresponding current inflow compensates for the boundary current as required by the number and chirality of the edge modes listed in Table I.

TABLE III. Net Goldstone-Wilczek current in units of $\frac{E_1}{2\pi}$. The current is obtained by taking into account the windings of different flavors as listed in Table II.

$2 > ma > 0$	$4 > ma > 2$	$6 > ma > 4$	$ma > 6$
1	-2	1	0

In this subsection, I will allow $m_1 \neq m_2$ while holding $\delta m_1 = \delta m_2 = 0$ and analyze the spectrum of the 16 different flavors in the Lagrangian of Eq. (3.22) for $R = a$. I define

$$\begin{aligned} a\tilde{\phi}_1 &= a\phi_1 - 2\delta_{i,1} - 2\delta_{j,1} - 2\delta_{k,1}, \\ a\tilde{\phi}_2 &= a\phi_2 - 2\delta_{i,1} - 2\delta_{j,1} - 2\delta_{l,1}. \end{aligned} \tag{3.33}$$

Note that $\tilde{\phi}_1$ and $\tilde{\phi}_2$ act as gaps for the different flavors and are constants away from the domain wall in ϕ_1 and ϕ_2. More specifically, the gap for a particular flavor is given by $\sqrt{\tilde{\phi}_1^2 + \tilde{\phi}_2^2}$. It is interesting to explore the behavior of the gap and its variation in space as one changes the parameters in the theory. With $2 > am_1 > 0$, the gap $a\tilde{\phi}_1$ passes through zero along the $x^2 = 0$ domain wall, for two of the flavors $\psi_{0,0,0,0}$ and $\psi_{0,0,0,1}$. For the other 14 flavors $\tilde{\phi}_1$ does not pass through zero anywhere in space as long as $2 > am_1 > 0$. If I now consider the behavior of $a\tilde{\phi}_2$, I find that for all values of am_2, $a\tilde{\phi}_2$ for the flavor $\psi_{0,0,0,0}$ is nonzero along the entire $x^2 = 0$ domain wall, except at the point $x^3 = 0$. The situation for the other flavor $\psi_{0,0,0,1}$ is slightly different. For $0 < am_2 < 2$, $a\tilde{\phi}_2$ for $\psi_{0,0,0,1}$ is nonzero in all of space. When $am_2 = 2$, however, $a\tilde{\phi}_2$ passes through zero, along the $x^3 > 0$ surface of the domain wall at $x^2 = 0$. Therefore the spectrum of the $\psi_{0,0,0,1}$ flavor goes gapless along a half-plane of the domain wall at $x_2 = 0$ when $am_2 = 2$. As $am_2 > 0$, the gap for this flavor passes through zero only at $x^2 = 0$, $x^3 = 0$ just as in the case of the flavor $\psi_{0,0,0,0}$. $a\tilde{\phi}_1$ and $a\tilde{\phi}_2$ does not pass through zero for any of the other flavors for $2 > am_1 > 0$. As I increase am_1, several other flavors go gapless along the positive half of the domain wall at $x_2 = 0$ as am_2 reaches 2, 4, and 6. In Table IV I show for which flavors the gap passes through zero along the entire $x^3 > 0$ region of the domain wall at $x^2 = 0$. A similar analysis can be done for the domain wall at $x^3 = 0$ where the gaps for the different flavors will pass through zero when am_1 reaches 2, 4, and 6 for various values of am_2. Note that, the appearance of this surface along which the gap for certain flavors goes to zero coincides with the boundaries of the regions containing chiral edge states in Fig. 2. Since fermion gap closing is typically associated with phase transitions, we can expect the boundaries in Fig. 2 to correspond to phase transitions as well.

IV. DISCUSSION

A. Vortex configuration

Although the crossed domain wall configuration and the vortex axion string carry the same winding and the spectrum of massless states are analogous, the details of the two systems differ. In particular, the range of the Wilson parameters and the gaps ϕ_1 and ϕ_2 for which one finds 1, 2,

TABLE IV. The flavors for which the gap passes through zero along a surface in the region $x^3 > 0$ at $x^2 = 0$ (along the domain wall) when $m_2 a = 2, 4, 6$.

	$2 > m_1 a > 0$	$4 > m_1 a > 2$	$6 > m_1 a > 4$	$m_1 a > 6$
$m_2 a = 2$	$\psi_{0,0,0,1}$	$\psi_{1,0,0,0}, \psi_{0,1,0,0}, \psi_{0,0,0,1}, \psi_{0,0,1,1}$	$\psi_{1,0,0,0}, \psi_{0,1,0,0}$ $\psi_{0,0,0,1}, \psi_{1,0,1,0}$, $\psi_{0,1,1,0}, \psi_{0,0,1,1}$	$\psi_{1,0,0,0}, \psi_{1,0,1,0}$ $\psi_{0,1,0,0}, \psi_{0,1,1,0}$ $\psi_{0,0,0,1}, \psi_{0,0,1,1}$
$m_2 a = 4$	✗	$\psi_{1,0,0,1}, \psi_{0,1,0,1}$	$\psi_{1,0,0,1}, \psi_{0,1,0,1}$ $\psi_{1,0,1,1}, \psi_{0,1,1,1}$ $\psi_{1,1,0,0}$	$\psi_{1,1,0,0}, \psi_{1,1,1,0}$ $\psi_{1,0,0,1}, \psi_{1,0,1,1}$ $\psi_{0,1,0,1}, \psi_{0,1,1,1}$
$m_2 a = 6$	✗	✗	$\psi_{1,1,0,1}$	$\psi_{1,1,0,1}, \psi_{1,1,1,1}$

and 1 chiral edge states on the defect, corresponding to the 4 different doublers, is expected to be different for the crossed domain wall defect and the vortex. Moreover, the radial profile for the edge states in the discretized vortex configuration will be different from the radial profile obtained for the crossed domain wall configuration. The difference in the radial profile will arise from the fact that the variation in ϕ_1 and ϕ_2 in a vortex configuration is uniform in all of space as opposed to that in a crossed domain wall where ϕ_1 and ϕ_2 change rather rapidly along two surfaces while remaining constant in the rest of the bulk. Similarly, in a vortex configuration one will find surfaces along which the gap corresponding to different flavors will pass through zero in analogy with the discussion in Sec. III B. Of course, the range of the parameters for which the gap will pass through zero will be different from those obtained in Table IV.

B. Finite volume lattice construction

The construction of discretized axion string edge states pursued in this paper applies to infinite volume lattices. It would be interesting to implement this construction numerically which will inevitably involve a finite volume lattice. Since it would be impossible to create a single vortex of winding one in a box, one can consider a vortex and an antivortex or a vortex loop geometry so that there is no net winding in the system. The vortex and the antivortex will host chiral edge states of opposite chirality. The number of these chiral edge states will of course depend on the ratio of the scalar vacuum expectation value to that of the Wilson parameter. This finite volume system will have a net zero chirality. The edge states will acquire a mass which is going to be exponentially suppressed in the distance between the vortex and the antivortex or the size of the axion loop.

Implementing the crossed domain wall configuration in a finite volume, on the other hand will involve two vortices and two antivortices corresponding to a wall and an antiwall in x_2 and x_3. The crossed domain wall configurations in question are $\phi_1 = m_1(\epsilon(x_2) + \epsilon(L - x_2))$, $\phi_2 = m_2(\epsilon(x_3) + \epsilon(L - x_3))$, such that the domain wall and antidomain walls are at a distance L apart. If the defects at $\{x_2 = 0, x_3 = 0\}$ and $\{x_2 = L, x_3 = L\}$ carry a winding of 1 in $\phi_1 + i\phi_2$, the ones at $\{x_2 = 0, x_3 = L\}$ and $\{x_2 = L, x_3 = 0\}$ carry a winding of -1. Then, these defects will carry chiral edge states with a net chiral imbalance provided m_1 and m_2 and the Wilson-like parameters are in the appropriate range as discussed in the paper. Locally near each of the crossed domain wall defects one will observe an inflowing or outflowing current depending on the number and chirality of zero modes on the defect.

C. Axion insulator

The continuum Callan-Harvey example of Dirac fermions coupled to an axion field has analogs in condensed matter systems known as axion insulators. To understand the connection consider the four band Weyl semimetal Hamiltonian discussed in [13]

$$H = v_F \sum_{i=1}^{3} \Gamma^i(-i\partial_i - eA_i - q_i\Gamma) - eA_0, \qquad (4.1)$$

where Γ^i are Dirac matrices and Γ is the chirality operator with the Dirac space being constructed from spin and pseudospin degrees of freedom [32]. A^μ stands for the vector gauge field and q_i is a vector meant to shift the gapless points away from zero momentum. The Dirac matrices can be taken to be $\Gamma^i = \tau_3 \otimes \sigma_i$ and $\Gamma = \tau_3 \otimes \sigma_0$ with commutation relations $[\Gamma^i, \Gamma^j] = 2\delta^{ij}$ and $[\Gamma^i, \Gamma] = 0$. Setting the vector gauge field to zero, it is easy to see that the low energy spectrum consists of left-handed modes $\Gamma = +1$ with $H_+(\mathbf{k}) = +v_F\boldsymbol{\sigma}.(\mathbf{k} - \mathbf{q})$ and right-handed modes $\Gamma = -1$ with $H_-(\mathbf{k}) = -v_F\boldsymbol{\sigma}.(\mathbf{k} + \mathbf{q})$. The points $\mathbf{k} = \mathbf{q}$ and $\mathbf{k} = -\mathbf{q}$ are called Weyl points. Expanding momenta around the Weyl points, one ends up with the Hamiltonian of a free Dirac fermion with chiral symmetry. Interestingly, as described in [13], one can design four fermi interactions that couple these two Weyl points in such a way so as to drive dynamical chiral symmetry breaking which gaps out the spectrum. This is called axion insulator and the corresponding Hamiltonian can be written as

$$H = \begin{pmatrix} -i\boldsymbol{\sigma}\cdot\partial & \sigma_0\Delta \\ \sigma_0\Delta^* & i\boldsymbol{\sigma}\cdot\partial \end{pmatrix}, \tag{4.2}$$

where Δ is the auxiliary field whose expectation value drives spontaneous breaking of chiral symmetry. The similarity with Callan-Harvey's axion-fermion Lagrangian is now manifest. In the presence of a nonzero vacuum expectation value for Δ, its phase serves as the axion field. A vortex in Δ will then serve as an axion string. As outlined in [16] this can be engineered by turning on an axial gauge field $\mathbf{A}_5$ constructed using spin-orbit coupling which turns the Hamiltonian of (4.2) into

$$H = \begin{pmatrix} \sigma\cdot(-i\partial - \mathbf{A}_5) & \sigma_0\Delta \\ \sigma_0\Delta^* & \boldsymbol{\sigma}\cdot(i\partial - \mathbf{A}_5) \end{pmatrix}. \tag{4.3}$$

The corresponding effective Hamiltonian for the auxiliary field can be written using gauge invariance and resembles Hamiltonian of a charge 2 Abelian Higgs model

$$H_\Delta = |(\partial - 2\mathbf{A}_5)\Delta|^2 + \cdots. \tag{4.4}$$

Turning on a background axial magnetic field therefore creates vortex lines in Δ causing its phase to twist. This creates the axion string background of Callan-Harvey. Substituting the vortex background in the Hamiltonian of Eq. (4.2) one obtains chiral edge state solutions.

The construction of axion insulator described above mimics the physics of the Callan-Harvey continuum model. It will be interesting to construct axion insulator models which mimic the behavior of the lattice axion string analyzed in this paper. The model of axion string discussed in [16] can engineer n chiral fermions on the string by engineering a winding n vortex. The corresponding Hall current is n times the Hall current for a unit winding vortex. In the lattice axion string model constructed in this paper one does not need a winding two string to obtain two chiral fermions. A winding one vortex can gives rise to two chiral fermions as long as the Wilson parameter is adjusted to be within a certain range as discussed in previous sections of this paper. If axion insulators can be made to mimic the lattice axion string of this paper, then they will be able to support two chiral edge states and a Hall current of two units with a single winding vortex. Whether such a construction is realizable will be explored in future work.

V. CONCLUSION

In this paper I constructed a lattice description of axion strings coupled to fermions which in the continuum is known to exhibit chiral edge states. The construction is facilitated by deforming the vortex configuration to a crossed domain wall configuration, both of which carry a winding of 1 in the axion field. Naive discretization of space-time leads to the elimination of any net chirality on the string or the crossed domain wall core due to the presence of fermion doublers. This problem is similar to what is encountered in lattice domain wall systems where a Wilson term has to be introduced in order to engineer a net imbalance of right and left chiral edge states on the wall. Inspired by the domain wall fermion construction, I introduce Wilson-like terms in the axion string Lagrangian in order to obtain a net imbalance of right and left moving edge states on the string. As one changes the crossed domain wall height with respect to the Wilson-like parameter, one encounters discontinuous changes in the number of chiral fermions on the string. These changes are associated with the appearance of a two dimensional surface coinciding with the domain walls where the fermion gap passes through zero indicating a phase transition. In the presence of an electric field directed along the string, a Hall current flows from the bulk to the string. This Hall current jumps between different integers, exactly compensating for the boundary current as the number and chirality of the edge states change as a function of the parameters. This current is obtained by computing a one-loop Feynman diagram which integrates out the fermion away from the defect while treating the phase variation of the axion field and the background gauge field perturbatively. There are several interesting questions that remain to be explored. One of these involves implementing a finite volume numerical realization of both the crossed domain wall configuration and the vortex-loop configuration. It will also be interesting to explore a lattice model for the axion insulator mimicking the lattice quantum field theory described in this paper.

ACKNOWLEDGMENTS

I thank Thomas Iadecola and David B. Kaplan for useful discussions. This work was supported by the Department of Energy Nuclear Physics Quantum Horizons program through the Early Career Award DE-SC0021892.

[1] Curtis G. Callan, Jr. and Jeffrey A. Harvey, Anomalies and fermion zero modes on strings and domain walls, Nucl. Phys. **B250**, 427 (1985).
[2] Prateek Agrawal, Anson Hook, Junwu Huang, and Gustavo Marques-Tavares, Axion string signatures: A cosmological plasma collider, J. High Energy Phys. 01 (2022) 103.
[3] Prateek Agrawal, Anson Hook, and Junwu Huang, A CMB Millikan experiment with cosmic axiverse strings, J. High Energy Phys. 07 (2020) 138.
[4] Marco Gorghetto, Edward Hardy, and Giovanni Villadoro, Axions from strings: The attractive solution, J. High Energy Phys. 07 (2018) 151.
[5] Marco Gorghetto, Edward Hardy, and Giovanni Villadoro, More axions from strings, SciPost Phys. **10**, 050 (2021).
[6] Malte Buschmann, Joshua W. Foster, and Benjamin R. Safdi, Early-Universe Simulations of the Cosmological Axion, Phys. Rev. Lett. **124**, 161103 (2020).
[7] K. v. Klitzing, G. Dorda, and M. Pepper, New Method for High-Accuracy Determination of the Fine-Structure Constant Based on Quantized Hall Resistance, Phys. Rev. Lett. **45**, 494 (1980).
[8] D. J. Thouless, M. Kohmoto, M. P. Nightingale, and M. den Nijs, Quantized Hall Conductance in a Two-Dimensional Periodic Potential, Phys. Rev. Lett. **49**, 405 (1982).
[9] Joseph E. Avron and Ruedi Seiler, Quantization of the Hall Conductance for General, Multiparticle Schrödinger Hamiltonians, Phys. Rev. Lett. **54**, 259 (1985).
[10] Qian Niu, D. J. Thouless, and Yong-Shi Wu, Quantized Hall conductance as a topological invariant, Phys. Rev. B **31**, 3372 (1985).
[11] Akihiko Sekine and Kentaro Nomura, Axion electrodynamics in topological materials, J. Appl. Phys. **129**, 141101 (2021).
[12] Nicodemos Varnava and David Vanderbilt, Surfaces of axion insulators, Phys. Rev. B **98**, 245117 (2018).
[13] Zhong Wang and Shou-Cheng Zhang, Chiral anomaly, charge density waves, and axion strings from Weyl semimetals, Phys. Rev. B **87**, 161107 (2013).
[14] Zhong Wang and Shou-Cheng Zhang, Chiral anomaly, charge density waves, and axion strings from Weyl semimetals, Phys. Rev. B **87**, 161107 (2013).
[15] Xiao-Liang Qi, Edward Witten, and Shou-Cheng Zhang, Axion topological field theory of topological superconductors, Phys. Rev. B **87**, 134519 (2013).
[16] Thomas Schuster, Thomas Iadecola, Claudio Chamon, Roman Jackiw, and So-Young Pi, Dissipationless conductance in a topological coaxial cable, Phys. Rev. B **94**, 115110 (2016).
[17] David B. Kaplan, A method for simulating chiral fermions on the lattice, Phys. Lett. B **288**, 342 (1992).
[18] Karl Jansen, Chiral fermions and anomalies on a finite lattice, Phys. Lett. B **288**, 348 (1992).
[19] Maarten F. L. Golterman, Karl Jansen, and David B. Kaplan, Chern-Simons currents and chiral fermions on the lattice, Phys. Lett. B **301**, 219 (1993).
[20] Karl Jansen and Martin Schmaltz, Critical momenta of lattice chiral fermions, Phys. Lett. B **296**, 374 (1992).
[21] Xiao-Liang Qi, Taylor L. Hughes, and Shou-Cheng Zhang, Topological field theory of time-reversal invariant insulators, Phys. Rev. B **78**, 195424 (2008).
[22] B. Andrei Bernevig, Taylor L. Hughes, and Shou-Cheng Zhang, Quantum spin Hall effect and topological phase transition in HgTe quantum wells, Science **314**, 1757 (2006).
[23] David B. Kaplan and Srimoyee Sen, Index Theorems, Generalized Hall Currents, and Topology for Gapless Defect Fermions, Phys. Rev. Lett. **128**, 251601 (2022).
[24] David B. Kaplan and Srimoyee Sen, Generalized Hall currents in topological insulators and superconductors, 2022, arXiv:2205.05707.
[25] E. Tirrito, S. Hands, and A. Bermudez, Large-S and tensor-network methods for strongly-interacting topological insulators, Symmetry **14**, 799 (2022).
[26] L. Ziegler, E. Tirrito, M. Lewenstein, S. Hands, and A. Bermudez, Large-N Chern insulators: Lattice field theory and quantum simulation approaches to correlation effects in the quantum anomalous Hall effect, Ann. Phys. (Amsterdam) **439**, 168763 (2022).
[27] L. Ziegler, E. Tirrito, M. Lewenstein, S. Hands, and A. Bermudez, Correlated Chern insulators in two-dimensional Raman lattices: A cold-atom regularization of strongly-coupled four-Fermi field theories, 2020, arXiv:2011.08744.
[28] Srimoyee Sen, Chern insulator transitions with Wilson fermions on a hyperrectangular lattice, Phys. Rev. D **102**, 094520 (2020).
[29] David B. Kaplan and Srimoyee Sen, Fractional Quantum Hall Effect in a Relativistic Field Theory, Phys. Rev. Lett. **124**, 131601 (2020).
[30] Hidenori Fukaya, Tetsuya Onogi, Shota Yamamoto, and Ryo Yamamura, Six-dimensional regularization of chiral gauge theories, Prog. Theor. Exp. Phys. **2017**, 033B06 (2017).
[31] Jeffrey Goldstone and Frank Wilczek, Fractional Quantum Numbers on Solitons, Phys. Rev. Lett. **47**, 986 (1981).
[32] A. A. Burkov and Leon Balents, Weyl Semimetal in a Topological Insulator Multilayer, Phys. Rev. Lett. **107**, 127205 (2011).